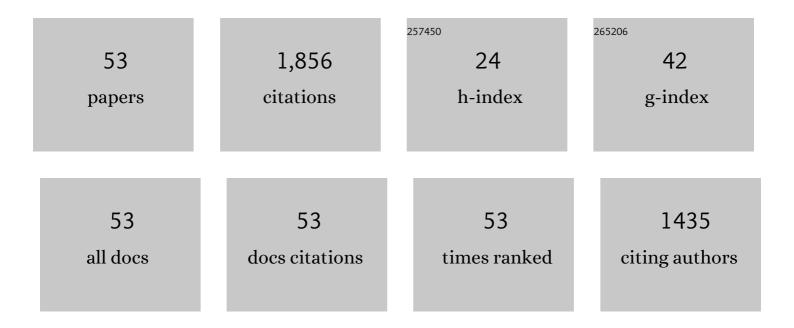
Ryosuke Sinmyo

List of Publications by Year in descending order

Source: https://exaly.com/author-pdf/382437/publications.pdf Version: 2024-02-01



#	Article	IF	CITATIONS
1	Crystallization of silicon dioxide and compositional evolution of the Earth's core. Nature, 2017, 543, 99-102.	27.8	161
2	The Electrical Conductivity of Post-Perovskite in Earth's D'' Layer. Science, 2008, 320, 89-91.	12.6	127
3	High Poisson's ratio of Earth's inner core explained by carbon alloying. Nature Geoscience, 2015, 8, 220-223.	12.9	113
4	Determination of post-perovskite phase transition boundary in MgSiO3using Au and MgO pressure standards. Geophysical Research Letters, 2006, 33, n/a-n/a.	4.0	94
5	Melting curve of iron to 290 GPa determined in a resistance-heated diamond-anvil cell. Earth and Planetary Science Letters, 2019, 510, 45-52.	4.4	81
6	The Soret diffusion in laser-heated diamond-anvil cell. Physics of the Earth and Planetary Interiors, 2010, 180, 172-178.	1.9	74
7	Partitioning of iron between perovskite/postperovskite and ferropericlase in the lower mantle. Journal of Geophysical Research, 2008, 113, .	3.3	73
8	Melting experiments on Fe–Fe 3 S system to 254 GPa. Earth and Planetary Science Letters, 2017, 464, 135-141.	4.4	73
9	Fate of MgSiO ₃ melts at core–mantle boundary conditions. Proceedings of the National Academy of Sciences of the United States of America, 2015, 112, 14186-14190.	7.1	72
10	Electrical conductivity of NaCl-bearing aqueous fluids to 600°C and 1ÂGPa. Contributions To Mineralogy and Petrology, 2017, 172, 1.	3.1	72
11	Effect of iron oxidation state on the electrical conductivity of the Earth's lower mantle. Nature Communications, 2013, 4, 1427.	12.8	60
12	The valence state and partitioning of iron in the Earth's lowermost mantle. Journal of Geophysical Research, 2011, 116, .	3.3	54
13	Perovskite in Earth's deep interior. Science, 2017, 358, 734-738.	12.6	54
14	Portable double-sided laser-heating system for Mössbauer spectroscopy and X-ray diffraction experiments at synchrotron facilities with diamond anvil cells. Review of Scientific Instruments, 2012, 83, 124501.	1.3	50
15	Discovery of Fe7O9: a new iron oxide with a complex monoclinic structure. Scientific Reports, 2016, 6, 32852.	3.3	50
16	Ferric iron in Al-bearing post-perovskite. Geophysical Research Letters, 2006, 33, .	4.0	44
17	Melting experiments on the Fe–C binary system up to 255 GPa: Constraints on the carbon content in the Earth's core. Earth and Planetary Science Letters, 2019, 515, 135-144.	4.4	43
18	Iron partitioning in pyrolitic lower mantle. Physics and Chemistry of Minerals, 2013, 40, 107-113.	0.8	42

RYOSUKE SINMYO

#	Article	IF	CITATIONS
19	Hydrogen Limits Carbon in Liquid Iron. Geophysical Research Letters, 2019, 46, 5190-5197.	4.0	42
20	Lower mantle electrical conductivity based on measurements of Al, Fe-bearing perovskite under lower mantle conditions. Earth and Planetary Science Letters, 2014, 393, 165-172.	4.4	41
21	Stability of Fe,Al-bearing bridgmanite in the lower mantle and synthesis of pure Fe-bridgmanite. Science Advances, 2016, 2, e1600427.	10.3	31
22	Oxidation state of the lower mantle: In situ observations of the iron electronic configuration in bridgmanite at extreme conditions. Earth and Planetary Science Letters, 2015, 423, 78-86.	4.4	30
23	Iron spin state in silicate perovskite at conditions of the Earth's deep interior. High Pressure Research, 2013, 33, 663-672.	1.2	27
24	The effect of iron and aluminum incorporation on lattice thermal conductivity of bridgmanite at the Earth's lower mantle. Earth and Planetary Science Letters, 2017, 474, 25-31.	4.4	25
25	The advanced ion-milling method for preparation of thin film using ion slicer: Application to a sample recovered from diamond-anvil cell. Review of Scientific Instruments, 2009, 80, 013901.	1.3	22
26	Melting experiments on Fe–Si–S alloys to core pressures: Silicon in the core?. American Mineralogist, 2018, 103, 742-748.	1.9	22
27	The spin state of Fe ³⁺ in lower mantle bridgmanite. American Mineralogist, 2017, 102, 1263-1269.	1.9	21
28	Electronic spin state of Fe,Al-containing MgSiO3 perovskite at lower mantle conditions. Lithos, 2014, 189, 167-172.	1.4	19
29	Ferric iron content in (Mg,Fe)SiO3 perovskite and post-perovskite at deep lower mantle conditions. American Mineralogist, 2008, 93, 1899-1902.	1.9	17
30	Phase transition boundary between fcc and hcp structures in Fe-Si alloy and its implications for terrestrial planetary cores. American Mineralogist, 2019, 104, 94-99.	1.9	17
31	Phase relations in the system Fe–Ni–Si to 200 GPa and 3900 K and implications for Earth's core. Earth and Planetary Science Letters, 2019, 512, 83-88.	4.4	17
32	Crystal chemistry of Fe3+-bearing (Mg, Fe)SiO3 perovskite: a single-crystal X-ray diffraction study. Physics and Chemistry of Minerals, 2014, 41, 409-417.	0.8	16
33	Iron spin state in silicate glass at high pressure: Implications for melts in the Earth's lower mantle. Earth and Planetary Science Letters, 2014, 385, 130-136.	4.4	16
34	The stability of Fe5O6 and Fe4O5 at high pressure and temperature. American Mineralogist, 2019, 104, 1356-1359.	1.9	16
35	Melting Experiments on Liquidus Phase Relations in the Feâ€Sâ€O Ternary System Under Core Pressures. Geophysical Research Letters, 2019, 46, 5137-5145.	4.0	16
36	Synthesis and crystal structure of LiNbO3-type Mg3Al2Si3O12: A possible indicator of shock conditions of meteorites. American Mineralogist, 2017, 102, 1947-1952.	1.9	14

RYOSUKE SINMYO

#	Article	IF	CITATIONS
37	A portable on-axis laser-heating system for near-90° X-ray spectroscopy: application to ferropericlase and iron silicide. Journal of Synchrotron Radiation, 2020, 27, 414-424.	2.4	14
38	Effect of spin transition of iron on the thermal conductivity of (Fe, Al)-bearing bridgmanite. Earth and Planetary Science Letters, 2019, 520, 188-198.	4.4	13
39	Melting Curve and Equation of State of βâ€Fe 7 N 3 : Nitrogen in the Core?. Journal of Geophysical Research: Solid Earth, 2019, 124, 3448-3457.	3.4	11
40	Siliconâ€Depleted Presentâ€Day Earth's Outer Core Revealed by Sound Velocity Measurements of Liquid Feâ€Si Alloy, Journal of Geophysical Research: Solid Earth, 2020, 125, e2020JB019399.	3.4	10
41	xmins:mml="http://www.w3.org/1998/Math/Math/MathML"> <mml:mrow><mml:mi mathvariant="normal">M<mml:msub><mml:mi mathvariant="normal">g<mml:mrow><mml:mn>1</mml:mn><mml:mo>–</mml:mo><mml:mi>xmathvariant="normal">F</mml:mi><mml:msub><mml:mi< td=""><td>nnal:eni></td><td><</td></mml:mi<></mml:msub></mml:mrow></mml:mi </mml:msub></mml:mi </mml:mrow>	nn al:e ni>	<
42	Sound velocities of skiagite–iron–majorite solid solution to 56ÂGPa probed by nuclear inelastic scattering. Physics and Chemistry of Minerals, 2018, 45, 397-404.	0.8	8
43	Experimental Determination of Eutectic Liquid Compositions in the MgOâ€SiO ₂ System to the Lowermost Mantle Pressures. Geophysical Research Letters, 2018, 45, 9552-9558.	4.0	8
44	Effect of Fe 3+ on Phase Relations in the Lower Mantle: Implications for Redox Melting in Stagnant Slabs. Journal of Geophysical Research: Solid Earth, 2019, 124, 12484-12497.	3.4	8
45	The influence of solid solution on elastic wave velocity determination in (Mg,Fe)O using nuclear inelastic scattering. Physics of the Earth and Planetary Interiors, 2014, 229, 16-23.	1.9	7
46	Sound velocities of bridgmanite from density of states determined by nuclear inelastic scattering and first-principles calculations. Progress in Earth and Planetary Science, 2016, 3, .	3.0	6
47	Discovery of Newâ€Structured Postâ€Spinel MgFe 2 O 4 : Crystal Structure and Highâ€Pressure Phase Relations. Geophysical Research Letters, 2020, 47, e2020GL087490.	4.0	6
48	Discovery of Elgoresyite, (Mg,Fe)5Si2O9: Implications for Novel Iron-Magnesium Silicates in Rocky Planetary Interiors. ACS Earth and Space Chemistry, 2021, 5, 2124-2130.	2.7	6
49	Anomalous compressibility in (Fe,Al)-bearing bridgmanite: implications for the spin state of iron. Physics and Chemistry of Minerals, 2020, 47, 1.	0.8	3
50	The electrical conductivity of Fe4O5, Fe5O6, and Fe7O9 up to 60 GPa. Physics and Chemistry of Minerals, 2022, 49, .	0.8	2
51	Melting Temperature of Iron Determined in an Internal-Resistance-Heated Diamond-Anvil Cell. Review of High Pressure Science and Technology/Koatsuryoku No Kagaku To Gijutsu, 2019, 29, 113-120.	0.0	Ο
52	Measurements of Electrical Conductivity of (Mg,Fe)SiO3 Post-Perovskite using Laser-Heated Diamond-Anvil Cell. Review of High Pressure Science and Technology/Koatsuryoku No Kagaku To Gijutsu, 2008, 18, 260-266.	0.0	0
53	Physical and chemical properties of the mantle minerals explored by high-pressure and high-temperature experiments. Ganseki Kobutsu Kagaku, 2019, 48, 36-45.	0.1	0